applied optics

Application of haze and transmittance standards to highly scattering materials: the case of transparent wood

Hui Chen,[1] Ilya Sychugov,[2,*] and Lars A. Berglund[1]

[1]Wallenberg Wood Science Center, Department of Fiber and Polymer Technology, KTH Royal Institute of Technology, 100 44 Stockholm, Sweden
[2]Department of Applied Physics, School of Engineering Sciences, KTH Royal Institute of Technology, 114 19 Stockholm, Sweden
*ilyas@kth.se

Received 24 November 2025; revised 23 February 2026; accepted 23 February 2026; posted 24 February 2026; published 11 March 2026

Accurate characterization of transmittance and haze of transparent composites, such as transparent wood (TW), is challenging due to strong light-scattering effects. Reported TW data in the literature, particularly haze values, show substantial variability, which can be largely attributed to experimental setup parameters originally developed for transparent plastics rather than for strongly scattering composites. Here, we analyze the sensitivity of integrating sphere-based characterization methods (according to ASTM D1003) to key experimental parameters and propose measurement conditions tailored for TW. We find that, for transmittance measurements, a large input port size (e.g., 19 mm) of an integrating sphere (150 mm in diameter) is required for collecting all the transmitted photons of a 15 mm thick TW sample. Using a small input port alone can lead to a transmittance underestimation of up to 25% (from 48% to 37% at 550 nm). We also show that a smaller sphere size (50 mm in diameter) with a fixed input port (10 mm) can erroneously yield a transmittance that is about half of the expected value. For haze measurements, inappropriate choices of experimental parameters, such as the output port size, may introduce significant systematic bias, resulting in substantially underestimated haze values (e.g., 86% instead of 96% for a 15 mm thick TW sample). The proposed integrating sphere setup with adjustable ports provides a robust and reliable approach for the optical characterization of highly scattering yet transparent materials.

https://doi.org/10.1364/AO.585799

1. INTRODUCTION

Transparent wood (TW) combines the favorable mechanical properties of eco-friendly cellulosic materials with high optical transmittance [1,2]. Owing to this unique combination, TW has attracted increasing interest as a new class of optical and engineering materials with potential applications in optical devices and structural components [3–6]. Accurate characterization of the optical properties (mainly transmittance and haze) of TW is therefore essential, particularly for both the fundamental understanding of light–matter interactions and establishing reliable structure–property relationships in strongly light-scattering systems.

Wood is a porous cellular material composed of tube-like cells oriented in parallel (see Fig. 1). The cell walls consist mostly of oriented cellulose nanofibrils embedded in a matrix of molecularly mixed phenolic lignin and amorphous hemicelluloses. During the fabrication of TW, most of the lignin is chemically removed to reduce light absorption, and the resulting pore space is infiltrated with a polymer whose refractive index (RI) closely matches that of cellulose. The interaction between light and TW is intrinsically complex due to the hierarchical and anisotropic structure of the wood reinforcement [7]. Light absorption, primarily originating from residual lignin, and light scattering, mainly caused by the RI mismatch between cellulose and polymer as well as remaining air voids, occur simultaneously [8,9].

In some studies, TW has been fabricated from wood substrates cut from the transverse direction of a tree stem [2,10,11], as shown in Fig. 1A. In this configuration, scattering of the transmitted light is largely isotropic; however, the mechanical properties of the resulting composites are severely compromised. Moreover, during transmittance/haze measurements, a fraction of the incident photons may propagate through the polymer-filled cell lumina without interacting with the wood cell walls, particularly in thin samples where the specimen thickness is shorter than the characteristic length of wood fibers or vessels. As a result, the measured optical properties may not fully represent the intrinsic light–matter interactions within the TW composite unless a mechanically relevant structure is considered.

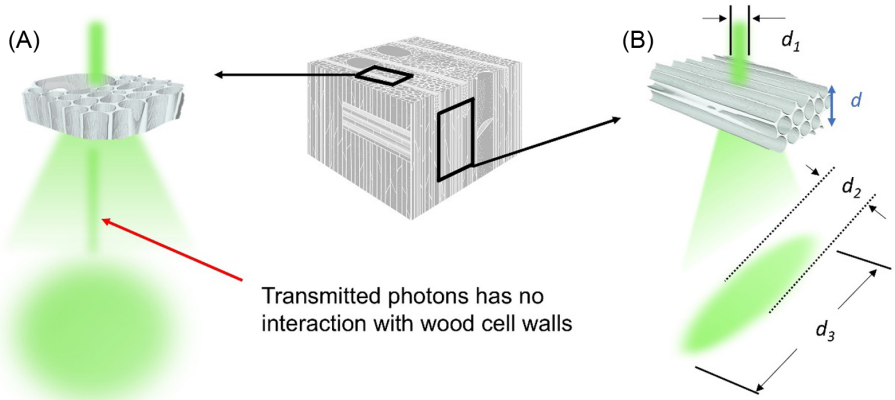

Fig. 1. Transparent wood (TW) made from (A) a wood substrate cut from the transverse direction of a tree stem and showing an isotropic scattering pattern (circular) for transmitted light, and from (B) a wood substrate cut from the longitudinal direction of a tree stem and showing an anisotropic scattering pattern (elliptical) for transmitted light. A collimated light beam with a diameter d_1 at the specimen input surface of TW (thickness d). d_2 (minor axis) and d_3 (major axis) are beam dimensions at the output surface.

For this reason, most TW reported in the literature is fabricated from wood substrates cut along the longitudinal direction of a tree stem [1,4,8,12,13], as shown in Fig. 1B. This configuration preserves favorable mechanical properties, as the wood fibers remain parallel to the specimen surface, while maintaining high optical transmittance. From an optical perspective, when an incident beam (with diameter d_1) propagates through a TW specimen (thickness d), all photons are expected to interact with the wood cell walls, since the diameter of individual wood cells is typically on the order of 30 μm (with vessels reaching up to around 300 μm), whereas TW thicknesses (d) generally exceed 0.5 mm. In this case, light scattering becomes inherently anisotropic due to the geometry and alignment of the tubular wood fibers [14]. Consequently, both the minor axis (d_2) and the major axis (d_3) of the transmitted beam at the output surface increase with the propagation distance beyond the sample, reflecting the direction-dependent scattering behavior of TW (Fig. 1B).

Despite the growing number of publications in this field, the quantitative comparison of optical properties reported by different laboratories remains difficult. This can be attributed to differences in the TW sample design as well as to variations in measurement methodology, particularly for highly scattering materials. First, from a materials perspective, a large majority of studies report optical data for only a single TW thickness, often fabricated from different wood species with varying wood content and cellular microstructures [11,15–18]. This heterogeneity significantly complicates cross-laboratory comparisons and limits the generality of conclusions drawn from individual data sets. Second, and more critically, differences in measurement methodology play a central role. Integrating sphere-based techniques are widely employed for transmittance and haze measurements; however, their accuracy depends strongly on sphere configuration, port geometry, wall reflectance, and incident beam conditions. The non-equivalence of different measurement procedures and sphere multipliers has been systematically analyzed from a metrological perspective [19], and subsequent studies have shown that these effects become more pronounced for highly scattering samples, leading to discrepancies between different measurement systems [20].

More recently, correction and compensation strategies have been proposed to improve the accuracy of diffuse transmittance and haze measurements, particularly for samples with high haze values [21]. For TW, many studies rely on the ASTM D1003 standard [22], which was originally developed for transparent materials with low light scattering. However, these standard measurement parameters (i.e., small integrating sphere diameter and fixed input and output ports) for low scattering materials may not be appropriate for highly scattering TW, especially for haze measurements. These challenges motivate a thorough examination of optical characterization methods for TW. In this work, we systematically investigate how the selection of experimental setup parameters influences optical property measurements of TW. Key factors that critically affect the accuracy of transmittance and haze measurements are identified, and optimized integrating sphere configurations are proposed for TW. The suggested protocol can be used not only for TW, but also for other highly scattering materials.

2. MATERIALS AND METHODS

A. Transparent Wood Fabrication

Diffusely porous wood species were selected for transparent wood (TW) fabrication following our previous procedure [9]. Briefly, natural wood veneers of beech and aspen (thickness: 0.5 mm, density: 660 and 410 kg/m^3, respectively), birch (thickness: 0.5 and 1 mm, density: 620 kg/m^3), and balsa (thickness: 1 and 4 mm, density: 120 kg/m^3) were used (purchased from Materials AB, Sweden). Delignification was performed in a 1 wt% $NaClO_2$ solution buffered at pH 4.6 at 80°C for 6 h, with the 4 mm balsa veneer treated for 10 h to ensure complete removal of lignin. Delignified templates were sequentially solvent exchanged from water to ethanol and finally to acetone, with each step repeated three times. Acetylation of the 1 mm delignified birch was carried out with acetic anhydride (Sigma-Aldrich) in N-methyl-2-pyrrolidone (NMP, Sigma-Aldrich) using pyridine (Sigma-Aldrich) as a catalyst [9,23].

All delignified and acetylated templates were vacuum impregnated with pre-polymerized methyl methacrylate (pre-MMA) and cured between glass slides at 70°C for 4 h to obtain TW composites. A 15 mm thick balsa TW was prepared as reported previously [24].

B. Transmittance and Haze Measurements

Angle-integrated total transmittance and haze were determined using a custom-built integrating sphere system, as shown in Fig. 2. The overall measurement principle follows ASTM D1003 [22]; however, certain experimental parameters were deliberately modified to accommodate the strong bulk scattering and anisotropic light propagation in TW. The illumination source was a laser-driven xenon plasma white-light source (Energetiq EQ-99) coupled with a monochromator (SP2150i, Princeton Instruments), providing an unpolarized light beam (to avoid the polarization effect from TW [25]), where the diameter of the beam (d_1) was further adjusted by an aperture and focused by a lens. The integrating sphere (with a diameter d_4 of 150 mm) employs a high-reflectance diffuse PTFE (Teflon) inner surface, offering approximately 99% reflectivity and near-Lambertian scattering over the visible-near infrared range, ensuring a uniform light field for optical measurements.

For transmittance measurements, the input light intensity (I_1) with no sample at the entrance port of the integrating sphere was first collected through an optical fiber at the bottom of the sphere connected to a detector. The input port of the sphere was equipped with interchangeable apertures (d_5), as shown in Fig. 2A. Next, the sample was placed at the entrance port of the integrating sphere, and the transmitted light intensity (I_2) was collected, as shown in Fig. 2B. Transmittance (T), which describes the fraction of the transmitted light intensity (I_2) in relation to the input light intensity (I_1) can be calculated through the following equation:

$$T = \frac{I_2}{I_1} \times 100\%. \tag{1}$$

Haze measurements were performed by opening the exit port (with adjustable size d_6 for tuning the deviation angle φ of the diffusely transmitted light from the incident beam), as shown in Fig. 2C. The background intensity (I_3) was recorded without the sample, followed by the measurement of the diffusely transmitted intensity (I_4) with the sample in place, as shown in Fig. 2D. Haze (H), which describes the fraction of diffused or scattered transmitted light intensity (I_4) relative to the total transmitted light intensity (I_2), can be obtained through

$$H = \left(\frac{I_4}{I_2} - \frac{I_3}{I_1}\right) \times 100\%. \tag{2}$$

For comparison, a smaller integrating sphere (internal diameter $d_4 = 50$ mm) with a fixed input port size ($d_5 = 10$ mm) was used. Measurements of transmittance and haze for each sample were performed for three times, and the data were averaged.

C. Anisotropic Scattering Profile of Transparent Wood

As a reference, we consider a non-scattering or very low scattering material, e.g., neat PMMA with $d = 15$ mm (Fig. 3A). Light can be transmitted without a change in direction, and one can see a leaf object clearly through PMMA, whether it is immediately on top (Fig. 3A$_1$) or 20 mm above the leaf (Fig. 3A$_2$), since scattering/haze is low. For TW with a thickness of 15 mm, as shown in Fig. 3B, the object under TW is blurred, whether it is directly attached (Fig. 3B$_1$) or 20 mm above the leaf (Fig. 3B$_2$), since TW shows high scattering/haze.

For thinner TW samples (e.g., 1 and 0.5 mm), we can see through the material clearly when the leaf is in direct contact with the TW sample (Figs. 3C$_1$–3H$_1$). When the samples are 20 mm above the leaf object, the image is again

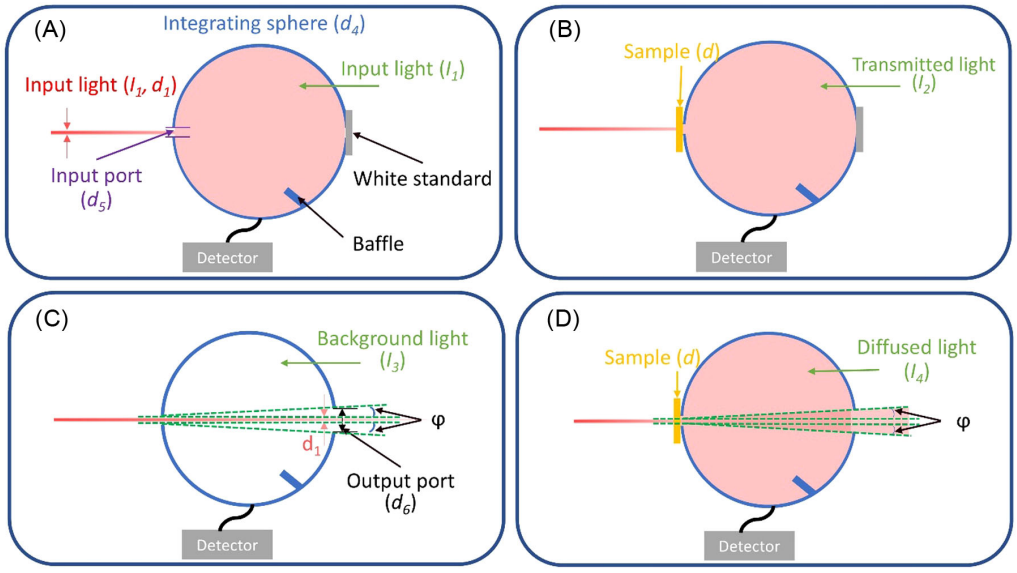

Fig. 2. Transmittance and haze measurements. Measurements of (A) the input light intensity (I_1), with no sample at the input port; (B) the transmitted light intensity (I_2) of a sample; (C) the scattered background light intensity (I_3) with no sample at the input port and the output port (d_6) open; and (D) the diffusely transmitted light intensity (I_4) for a sample (with the output port d_6 open). φ, the deviation angle from the incident beam.

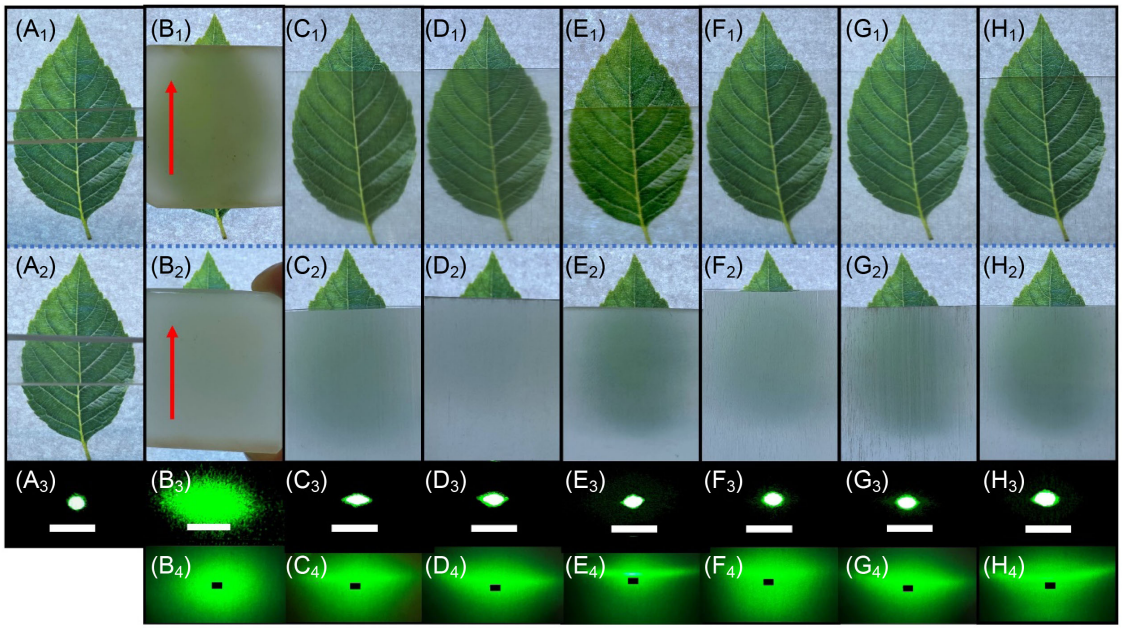

Fig. 3. Visual observation of the samples: (A) PMMA (15 mm), (B) balsa TW (15 mm), (C) balsa TW (1 mm), (D) birch TW (1 mm), (E) acetylated birch TW (1 mm), (F) beech TW (0.5 mm), (G) aspen TW (0.5 mm), and (H) birch TW (0.5 mm). For each sample, row 1, attached to a leaf; row 2, 20 mm above the leaf; row 3, the transmitted laser through the samples on a white paper screen attached to the exit surface (scale bar: 1 cm); and row 4, the transmitted laser through the samples on a white paper screen placed 20 mm behind the samples (scale bar: 1 cm). All the samples were placed with wood fibers in the red arrow direction.

blurred (Figs. 3C_2–3H_2). According to our previous research [8,9,14,24,26], the scattering originates from the refractive index (RI) mismatch between delignified wood (≈ 1.536) [26] and the polymer matrix (≈ 1.5 for PMMA), birefringence [27–30] of fibrous cellulose, optical defects from incomplete monomer impregnation, cellulose nanofibril aggregation, and air voids/gaps formed during polymerization. TW also shows anisotropic scattering [31], as shown in Fig. 1B, due to the alignment and geometry of tubular fibers. Rows 3 and 4 in Fig. 3 explain light scattering in a detailed way by showing images of a laser beam (Fig. 3A_3) transmitting through the samples. First, the visual appearances of the transmitted laser beam on a white paper screen attached to the exit surface of each sample are shown in Figs. 3B_3–3H_3. All the TW samples show slight scattering with an anisotropic pattern, except the high thickness TW (Fig. 3B_3), which already shows strong scattering. Thus, to collect all the transmitted photons during transmittance measurements, a larger input port opening (d_5 in Fig. 2) is needed, especially for high thickness samples, as shown in Fig. 3B. Further away from the sample exit surface (20 mm behind the sample) the paper screen reveals strong scattering with anisotropic patterns for all TWs (Figs. 3B_4–3H_4), which indicates high haze of the TW samples (note that all scale bars are 1 cm in Fig. 3, rows 3 and 4).

3. RESULTS

Most setups reported for TW optical properties (transmittance and haze) were UV–VIS spectrometers with an integrating sphere. The integrating sphere is normally small (i.e., 60 mm or smaller in diameter) [32], with fixed input and output port sizes. In addition, the beam size and the sample holder are often fixed and cannot be adjusted. Such instruments are suitable for low-scattering transparent plastics and thin films, but not necessarily for highly scattering materials. To address this problem, modified optical measurement techniques using adjustable integrating sphere setups are suggested.

A. Transmittance of Transparent Wood

The principle of an integrating sphere is to collect all the transmitted photons after numerous reflections inside it. The instrument can be described as a high numerical aperture detector [32–34]. If a TW sample is very thin or shows low scattering, as shown in Fig. 4A, the transmitted beam size at the output surface of TW (d_3, note that fibers in TW are oriented so that the major axis dimension d_3 is illustrated) is smaller than the input port size (d_5). All transmitted photons can be collected by the integrating sphere, which is ideal. In this case, even a luminance meter can be used for transmittance measurements of very thin wood-based composites [35]. However, the input beam diameter d_1 can obviously not be larger than the input port size d_5 since some photons will never enter the integrating sphere. Even if $d_1 = d_5$, it will cause erroneous measurements for a scattering material since the transmitted beam size d_3 at the output surface will be increased ($d_3 > d_5$), as shown in Fig. 4B (green part). This may seem trivial, but the mistake comes from neglecting the large extent of scattering in many TW composites.

In Fig. 4D, the problem is illustrated for the transmittance data of 1 mm thick balsa TW using two different light beam diameters ($d_1 = 2$ and 6 mm at the input port position, where $d_4 = 150$ and $d_5 = 6$ mm). The $d_1 = 6$ mm case has a slightly

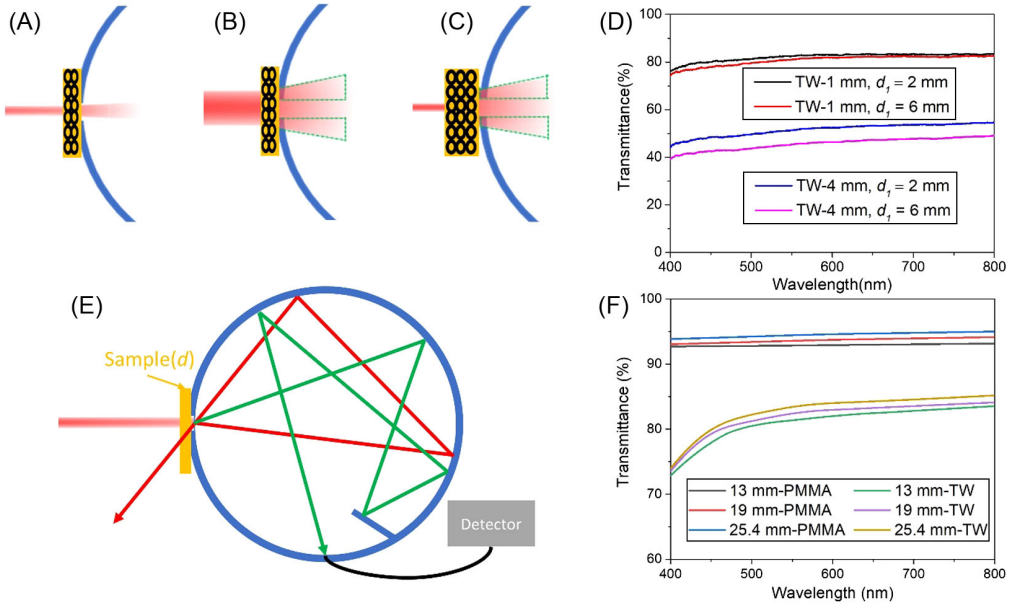

Fig. 4. (A) Thin or low scattering sample at the input port of an integrating sphere with the transmitted beam size smaller than the input port size ($d_3 < d_5$); (B) a thin or low scattering sample at the input port with an input beam size larger than or comparable to the input port ($d_1 \geq d_5$); (C) a highly scattering sample (high thickness or strong scattering) at the input port of the integrating sphere with an input beam size smaller than the input port size ($d_1 < d_5$) but a major axis of the transmitted beam size larger than the input port size ($d_3 > d_5$); (D) transmittance of TWs with two thicknesses measured with two different light beam diameters, respectively; (E) paths taken by transmitted photons inside the integrating sphere (green: collected by the detector; red: escaped from the input port of the integrating sphere); and (F) transmittance of PMMA and balsa TW (thickness 1 mm) measured with an integrating sphere ($d_4 = 150$ mm) with input port sizes of $d_5 = 13$, 19, and 25.4 mm, respectively.

lower transmittance compared with the $d_1 = 2$ mm case, although the difference is minor. For thicker TW samples with $d = 4$ mm, the transmittance is 45% in the $d_1 = 6$ mm case, but 51% when $d_1 = 2$ mm. Thus, the beam size d_1 should be small to achieve $d_3 < d_5$.

Another situation is that even if the beam size (d_1) is smaller than the input port size (d_5), as shown in Fig. 4C, for very thick samples, the discussed problem can lead to substantial deviations: very strong scattering may still result in a larger output beam size (d_3) compared with the integrating sphere input port (d_5) [5]. Besides this, TWs made from softwood or ring-porous hardwood may show a distinct annual ring structure, and a large beam size (d_1) is needed to make a more uniform coverage. In these cases, a large input port size (d_5) is needed. In some, papers or standards, it is clearly stated that the input port area should be at least two times larger than the input beam cross section [36,37].

If the size of the collimated input beam fulfills the condition described above (i.e., $d_1 = 6$ mm for TW with high thickness or a distinct annual ring structure), when the light has passed through the scattering specimen, as shown in Fig. 4E, the transmitted photons will be diffusely reflected many times at the internal surface of the integrating sphere (diameter d_4) and collected by the detector through the fiber (green photon path). However, some photons can escape (red photon path, Fig. 4E) through the input port (diameter d_5) [38]. This will decrease the number of collected photons by the integrating sphere, especially when d_5 is large for thick samples, and thus influence the measured transmittance. The ratio of d_5/d_4 therefore needs to be decreased to minimize this error (the fraction of escaped photons is shown in Fig. 4E, red path). According to the ASTM D1003 standard [22], the best performing integrating sphere should be any diameter (d_4) as long as the total input port area (S_{input}) does not exceed 4% of the internal reflecting area of the sphere ($S_{sphere\ effective}$). In the CIE15:2004 standard, this number was 10% [37].

Here, we tested the effect of the input port size ($d_5 = 13$, 19, and 25.4 mm for the integrating sphere with $d_4 = 150$ mm, corresponding to $S_{input}/S_{sphere\ effective} = 0.19\%$, 0.4%, and 0.72%, respectively) on the transmittance of a low-haze material (PMMA, 1 mm) and high-haze composites (balsa TW, 1 mm), and the data are shown in Fig. 4F. For PMMA with RI ≈ 1.5, based on the Fresnel reflection theory [39], around 4% of the input light is reflected from one surface under normal incidence. With this reasoning, the total reflectance is then $\sim 8\%$ from two surfaces (specular reflection also at the PMMA/air exit interface) and the transmittance should be around 92%. As shown in Fig. 4F, when the input port diameter (d_5) increased from 13 to 19 mm, transmittance at 550 nm increased from 92.8% to 93.6%, and further to 94.4% for $d_5 = 25.4$ mm. This is a manifestation of the "substitutional error" in the integrating sphere measurements.

Some reported transmittance data for amorphous polymers (e.g., PMMA) are higher than 92% [6,11,17,23,40,41], which can be due to the size of the input port, as illustrated here. For TW with $d = 1$ mm, transmittance at the wavelength of 550 nm shows a similar trend, where 81.4% for $d_5 = 13$ mm, 82.3% for $d_5 = 19$ mm, and 83.2% for $d_5 = 25.4$ mm. Although the size of d_5 had some influence on the total transmittance of both PMMA and TW, the variation was less than 2%,

indicating that most transmitted light was collected and that the measurement geometry was appropriate.

We proceed to test these guidelines for thick TW with $d = 15$ mm, where the setup details for optical transmittance measurements are more critical (Fig. 4C). For comparison, we first tested with a small integrating sphere ($d_4 = 50$ mm) with a fixed input port size ($d_5 = 10$ mm) and a collimated input beam size of $d_1 = 6$ mm. The transmittance is the lowest, as shown in Fig. 5A (green curve). Here, part of the transmitted light beam is blocked since it has $d_3 > 10$ mm due to large scattering in a thick sample ($d_3 > d_5$, Figs. 3B and 4C). Thus, the input port size d_5 needs to be increased, as well as the sphere size d_4. The blue curve in Fig. 5A is the transmittance measured with the input port size of $d_5 = 13$ mm for the large integrating sphere ($d_4 = 150$ mm), it increased from around 37% at 550 nm to around 48% for the $d_5 = 19$ mm case (red curve in Fig. 5A). This means that the input port size $d_5 = 13$ mm is still too small for such a thick TW sample. However, the transmittance for $d_5 = 25.4$ mm (black curve in Fig. 5A) is close to the $d_5 = 19$ mm case, which proves that the transmitted light beam size (d_3) is already smaller than the input port for $d_5 = 19$ mm, and all transmitted photons are collected by the integrating sphere for reliable data (results converging).

B. Haze of Transparent Wood

To illustrate the influence of setup parameters on haze measurements, the 15 mm thick TW specimen was characterized with collimated incident light ($d_1 = 6$ mm, which is circular, sharply defined, concentric within the light output port, and identical to that used for transmittance measurements in Fig. 5A), the input port size $d_5 = 19$ mm for the integrating sphere ($d_4 = 150$ mm), and an output port size $d_6 = 13$, 15, and 18 mm, respectively. The results shown in Fig. 5B show a lower haze value for $d_6 = 18$ mm (blue curve, around 86% at 550 nm), while it is higher for $d_6 = 15$ mm (Fig. 5B, red curve, around 92% at 550 nm) and 13 mm (Fig. 5B, black curve, around 96% at 550 nm) cases. The lowest diameter of the output port aperture ($d_6 = 13$ mm) yields the most accurate results here since it is calculated through the expression $d_1 + 2 \cdot d_4 \cdot \tan(1.3°)$ according to ASTM D1003. A haze value of 96% approaches the regime of complete loss of information, as expected for such thick samples under direct visual observation (Fig. 3B). The lower haze values observed for $d_6 = 15$ and 18 mm can be attributed to the fact that the deviation angle φ of the collected transmitted light exceeds the ASTM defined limit of 1.3° from the incident beam. As a result, part of the scattered light is incorrectly classified as specular transmission, leading to an underestimation of the haze. For this reason, erroneously low haze values have been reported in the literature [1,9,35].

By using these parameters for the integrating sphere ($d_4 = 150$ mm, $d_5 = 19$ mm, and $d_6 = 13$ mm combined with a collimated light beam $d_1 = 6$ mm), haze of TWs (from Figs. 3C–3H) made from various wood species with different thicknesses was measured, as shown in Fig. 5C. All TWs, even those with very low thickness (0.5 mm) show very high scattering with haze values $\geq 90\%$. Although acetylation treatment of the wood substrate can reduce scattering, the haze data for acetylated birch TW of thickness 1 mm are still very high ($\approx 84\%$ at 550 nm, green curve in Fig. 5C). This is in qualitative agreement with Fig. 3, row 2, where information behind the TW samples is lost due to strong scattering. This shows that the integrating sphere protocol suggested here provides more accurate haze measurements of TW materials in a range of thicknesses and scattering properties.

To verify and calibrate our suggested configuration in a broader range of haze values, calibrated haze plates were measured using the above parameters. The results (haze at 550 nm) for each haze plate are shown in Table 1, where the haze measured with the output port apertures of 15 and 18 mm shows lower values compared with the 13 mm aperture. In addition, the results from the 13 mm output port aperture agree with the calibrated values (within 6% deviation) from the vendor, confirming the identification of the correct output port aperture in relation to the beam size used for TW in this work.

4. SUMMARY OF THE PROPOSED PROTOCOL

According to the discussion in Section 3, we conclude that both the geometries of TW specimens and integrating sphere need to be correctly selected to provide representative data and summarize the introduced modifications below:

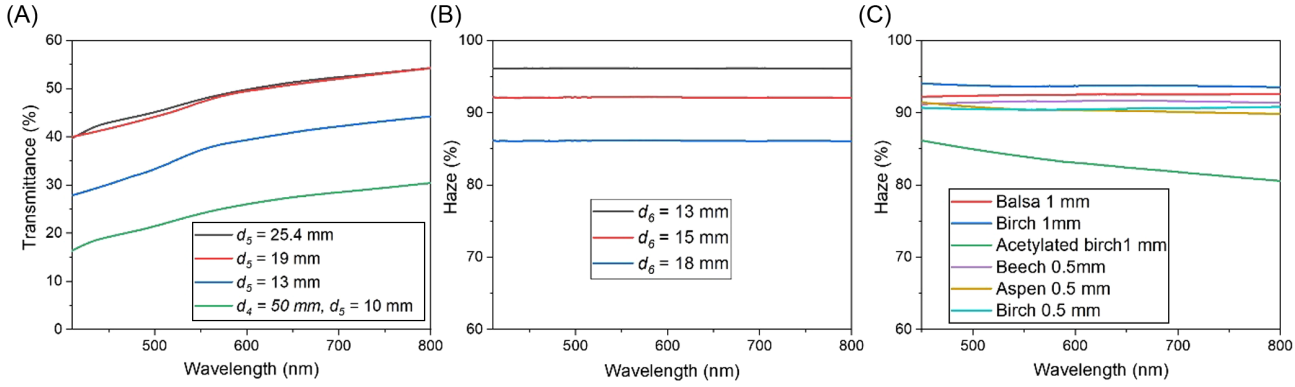

Fig. 5. (A) Transmittance of 15 mm thick TW measured using a 50 mm integrating sphere with a fixed input port size of 10 mm, and three different input port apertures for the 150 mm integrating sphere; (B) haze of 15 mm thick TW measured using three different output port apertures of the 150 mm integrating sphere; and (C) haze of TWs from Fig. 3, with different wood species and thicknesses, measured with the output port size $d_6 = 13$ mm.

Table 1. Haze (at 550 nm) of Calibrated Haze Plates Measured with Three Output Port Apertures of the Integrating Sphere

Calibrated Haze Plates (%)	Output Port Size 13 mm (%)	Output Port Size 15 mm (%)	Output Port Size 18 mm (%)
9.10 (10)	9.6	8.8	8.4
16.52 (20)	17.2	15.4	14.2
26.99 (30)	27.7	25.6	23.5

1. for transmittance measurements, the heterogeneous (e.g., distinct annual ring structure) must be taken into account to ensure that the data are representative by selecting a suitable beam size d_1. Furthermore, the diameter of the input port of the integrating sphere (d_5) should be larger than the transmitted beam size d_3, so that all transmitted photons can reach the integrating sphere. In addition, the diameter of the integrating sphere (d_4) must be large enough to fulfill a low ratio of d_5/d_4. Otherwise, a substantial fraction of photons inside the sphere will escape through d_5;
2. and for haze measurements, an adjustable output port size (d_6) is required according to the beam size (d_1) and the diameter of the integrating sphere (d_4), to ensure that transmitted photons with a deviation angle larger than 1.3° from the incident beam direction are collected accurately. Some UV–VIS spectrometers have separate port reducers for the integrating sphere, but must be calibrated and chosen correctly for haze measurements of highly scattering materials.

5. CONCLUSION

ASTM D1003 has been widely adopted in previous studies for measuring transmittance and haze of transparent wood (TW). However, when experimental setup parameters originally developed for transparent plastics (e.g., small integrating spheres, fixed input and output port apertures in relation to the applied beam size) are directly applied to highly scattering materials such as TW composites, significant measurement biases may arise, particularly for thicker samples. Consequently, optical data reported in the literature, especially for haze values, are often difficult to interpret and compare quantitatively.

In the present study, we examine the sensitivity of integrating sphere-based optical measurements to key setup parameters for highly scattering materials, including both transmittance and haze. For TW, practical guidelines for accurate characterization are established by modifying critical parameters of the integrating sphere configuration. We show that optical transmittance strongly depends on the beam diameter, the input port aperture size, and the diameter of the integrating sphere, with these effects becoming increasingly pronounced for thick TW samples. Reliable transmittance data therefore require careful and consistent selection of these parameters.

Haze measurements are even more sensitive to experimental geometry and require particular attention to the choice of the output port aperture. The measured haze values confirm that TW exhibits strong light scattering, originating from its two-phase composite microstructure and defects formed during fabrication. These pronounced scattering properties make TW attractive for optical applications such as light diffusers. Conversely, for material design aimed at reducing haze, strategies such as using polymers with a refractive index more closely matched to the wood reinforcement can be employed.

The measurement guidelines proposed here are not limited to TW but are also applicable to other highly scattering materials. By minimizing methodology-related errors, more reliable comparisons of fabrication approaches and materials systems can be achieved.

Funding. European Commission (101138191); Knut and Alice Wallenberg Foundation (2021.0311); Swedish Research Council for Environment Agricultural Sciences and Spatial Planning (Formas) (2022-01231).

Acknowledgment. The AI-TranspWood project, HORIZON-CL4-2023-RESILIENCE-01-23, is gratefully acknowledged. This project is co-funded by the European Union. However, the views and opinions expressed are those of the author(s) only and do not necessarily reflect those of the European Union or HaDEA. Neither the European Union nor the granting authority can be held responsible for them. Funding from KTH and the Knut and Alice Wallenberg Foundation (Dnr 2021.0311) and Formas (2022-01231) is also acknowledged.

Disclosures. The authors declare no conflicts of interest.

Data availability. Data underlying the results presented in this paper are not publicly available at this time but may be obtained from the authors upon reasonable request.

REFERENCES

1. Y. Li, Q. Fu, S. Yu, *et al.*, "Optically transparent wood from a nanoporous cellulosic template: combining functional and structural performance," Biomacromolecules **17**, 1358–1364 (2016).
2. M. Zhu, J. Song, T. Li, *et al.*, "Highly anisotropic, highly transparent wood composites," Adv. Mater. **28**, 5181–5187 (2016).
3. A. W. Lang, Y. Li, M. D. Keersmaecker, *et al.*, "Transparent wood smart windows: polymer electrochromic devices based on poly(3,4-ethylenedioxythiophene):poly(styrene sulfonate) electrodes," ChemSusChem **11**, 854–863 (2018).
4. Y. Li, M. Cheng, E. Jungstedt, *et al.*, "Optically transparent wood substrate for perovskite solar cells," ACS Sustain. Chem. Eng. **7**, 6061–6067 (2019).
5. Y. Li, E. Vasileva, I. Sychugov, *et al.*, "Optically transparent wood: recent progress, opportunities, and challenges," Adv. Opt. Mater. **6**, 1800059 (2018).
6. X. Wang, T. Zhan, Y. Liu, *et al.*, "Large-size transparent wood for energy-saving building applications," ChemSusChem **11**, 4086–4093 (2018).
7. T. Nilsson and R. Rowell, "Historical wood - structure and properties," J. Cult. Herit. **13**, S5–S9 (2012).
8. H. Chen, C. Montanari, R. Shanker, *et al.*, "Photon walk in transparent wood: scattering and absorption in hierarchically structured materials," Adv. Opt. Mater. **10**, 2102732 (2022).
9. H. Chen, A. Baitenov, Y. Li, *et al.*, "Thickness dependence of optical transmittance of transparent wood: chemical modification effects," ACS Appl. Mater. Interfaces **11**, 35451–35457 (2019).
10. M. Zhu, T. Li, C. S. Davis, *et al.*, "Transparent and haze wood composites for highly efficient broadband light management in solar cells," Nano Energy **26**, 332–339 (2016).
11. H. Li, X. Guo, Y. He, *et al.*, "A green steam-modified delignification method to prepare low-lignin delignified wood for thick, large highly transparent wood composites," J. Mater. Res. **34**, 932–940 (2019).
12. A. Samanta, H. Chen, P. Samanta, *et al.*, "Reversible dual-stimuli-responsive chromic transparent wood biocomposites for smart window applications," ACS Appl. Mater. Interfaces **13**, 3270–3277 (2021).

13. C. Montanari, Y. Li, H. Chen, *et al.*, "Transparent wood for thermal energy storage and reversible optical transmittance," ACS Appl. Mater. Interfaces **11**, 20465–20472 (2019).
14. E. Vasileva, H. Chen, Y. Li, *et al.*, "Light scattering by structurally anisotropic media: a benchmark with transparent wood," Adv. Opt. Mater. **6**, 1800999 (2018).
15. R. Mi, C. Chen, T. Keplinger, *et al.*, "Scalable aesthetic transparent wood for energy efficient buildings," Nat. Commun. **11**, 3836 (2020).
16. C. Jia, C. Chen, R. Mi, *et al.*, "Clear wood toward high-performance building materials," ACS Nano **13**, 9993–10001 (2019).
17. C. Montanari, Y. Ogawa, P. Olsén, *et al.*, "High performance, fully bio-based, and optically transparent wood biocomposites," Adv. Sci. **8**, 2100559 (2021).
18. Y. Li, Q. Fu, R. Rojas, *et al.*, "Lignin-retaining transparent wood," ChemSusChem **10**, 3445–3451 (2017).
19. H. Yu and C. Hsaio, "Comparison of different measurement methods for transmittance haze," Metrologia **46**, S233–S237 (2009).
20. W. C. Liu, J. Hwang, A. Koo, *et al.*, "APMP pilot study on transmittance haze," J. Phys. Conf. Ser. **972**, 012023 (2018).
21. W. C. Liu and H. L. Yu, "Applicability of DIN 5036-3 to transmittance haze measurement," J. Phys. Conf. Ser. **2149**, 012011 (2022).
22. ASTM, "Standard test method for haze and luminous transmittance of transparent plastics," D1003-13 (ASTM International, 2013), pp. 1–7.
23. Y. Li, X. Yang, Q. Fu, *et al.*, "Towards centimeter thick transparent wood through interface manipulation," J. Mater. Chem. A **6**, 1094–1101 (2018).
24. H. Chen, J. Garemark, L. Li, *et al.*, "Green nanotechnology of cell wall swelling for nanostructured transparent wood of high optical performance," Small **21**, 2406749 (2024).
25. E. Vasileva, A. Baitenov, H. Chen, *et al.*, "Effect of transparent wood on the polarization degree of light," Opt. Lett. **44**, 2962–2965 (2019).
26. H. Chen, C. Montanari, M. Yan, *et al.*, "Refractive index of delignified wood for transparent biocomposites," RSC Adv. **10**, 40719–40724 (2020).
27. K. R. K. Iyer, P. Neelakantan, and T. Radhakrishnan, "Birefringence of native cellulosic fibers. I. Untreated cotton and ramie," J. Polym. Sci. Part A-2 Polym. Phys. **6**, 1747–1758 (1968).
28. K. Uetani, S. Izakura, T. Kasuga, *et al.*, "Self-alignment sequence of colloidal cellulose nanofibers induced by evaporation from aqueous suspensions," Colloids Interfaces **2**, 71 (2018).
29. E. D. Cranston and D. G. Gray, "Birefringence in spin-coated films containing cellulose nanocrystals," Colloids Surfaces A Physicochem. Eng. Asp. **325**, 44–51 (2008).
30. A. Dufresne, *Nanocellulose: From Nature to High Performance Tailored Materials* (Walter de Gruyter GmbH & Co KG, 2017).
31. R. Shanker, M. Hoglund, H. Chen, *et al.*, "Spatiotemporally resolved light propagation in transparent wood," Adv. Opt. Mater. **13**, e01789 (2025).
32. SHIMADZU, "Integrating spheres," https://www.shimadzu.com/an/service-support/technical-support/uv/essential_knowledge/integratingspheres.html.
33. R. E. Bennett and T. A. Hoyt, "Theory, construction and use of the photometric integrating sphere," in *Bureau of Standards* (US Department of Commerce, 1922), Vol. **18**, pp. 281–325.
34. L. M. Hanssen and K. A. Snail, "Integrating spheres for mid- and near-infrared reflection spectroscopy," in *Handbook of Vibrational Spectroscopy* (Wiley, 2002), Vol. **2**, pp. 1175–1192.
35. A. Vashistha, Y. Karout, M. C. Trouy, *et al.*, "Study of transmission and haze of translucent wood based on wood density and hyperspectral analysis of wood fabrication," ACS Appl. Opt. Mater. **3**, 42–53 (2024).
36. A. Höpe, "Diffuse reflectance and transmittance," in *Experimental Methods in the Physical Sciences* (Academic, 2014), Vol. **46**, pp. 179–219.
37. CIE, "Colorimetry," CIE15:2004 (International Commission on Illumination, 2004).
38. A. Tirpak and R. Young, "Accurate transmission measurements of translucent materials," (2024). https://www.photonics.com/Articles/Accurate_Transmission_Measurements_of_Translucent/a32297.
39. H. A. Cobb and F. H. Perrin, *The Principles of Optics* (McGraw-Hill, 1932).
40. J. Wu, Y. Wu, F. Yang, *et al.*, "Impact of delignification on morphological, optical and mechanical properties of transparent wood," Compos. Part A Appl. Sci. Manuf. **117**, 324–331 (2019).
41. Q. Fu, M. Yan, E. Jungstedt, *et al.*, "Transparent plywood as a load-bearing and luminescent biocomposite," Compos. Sci. Technol. **164**, 296–303 (2018).